Estudos em Ciências Exatas e da Terra

Desafios, Avanços e Possibilidades

Alireza Mohebi Ashtiani
(organizador)

VOL II

EDITORA ARTEMIS
2024

Estudos em Ciências Exatas e da Terra

Desafios, Avanços e Possibilidades

Alireza Mohebi Ashtiani
(organizador)

VOL II

EDITORA ARTEMIS
2024

Editora Chefe	Profª Drª Antonella Carvalho de Oliveira
Editora Executiva	M.ª Viviane Carvalho Mocellin
Direção de Arte	M.ª Bruna Bejarano
Diagramação	Elisangela Abreu
Organizador	Prof. Dr. Alireza Mohebi Ashtiani
Imagem da Capa	Abstract Style Landscapes /123RF
Bibliotecário	Maurício Amormino Júnior – CRB6/2422

EDITORA ARTEMIS
2024

Editora Artemis
Curitiba-PR Brasil
www.editoraartemis.com.br
e-mail:publicar@editoraartemis.com.br

Editora Artemis
Curitiba-PR Brasil
www.editoraartemis.com.br
e-mail:publicar@editoraartemis.com.br

Dados Internacionais de Catalogação na Publicação (CIP)
(eDOC BRASIL, Belo Horizonte/MG)

E82 Estudos em Ciências Exatas e da Terra: Desafios, Avanços e Possibilidades II / Organizador Alireza Mohebi Ashtiani. – Curitiba, PR: Artemis, 2024.

Formato: PDF
Requisitos de sistema: Adobe Acrobat Reader
Modo de acesso: World Wide Web
Inclui bibliografia
Edição bilíngue
ISBN 978-65-81701-39-0
DOI 10.37572/EdArt_271124390

1. Ciências exatas e da terra – Pesquisa – Brasil. I. Ashtiani, Alireza Mohebi.

CDD 509

Elaborado por Maurício Amormino Júnior – CRB6/2422

EDITORA ARTEMIS
2024

Editora Artemis
Curitiba-PR Brasil
www.editoraartemis.com.br
e-mail:publicar@editoraartemis.com.br

INTRODUÇÃO

A coletânea *Estudos em Ciências Exatas e da Terra: Desafios, Avanços e Possibilidades II* reúne contribuições significativas nas áreas de geociências, engenharia e física, com um foco particular na análise e solução de problemas complexos em diferentes contextos e regiões do mundo. Os artigos apresentados neste volume abordam desde questões geológicas e ambientais até modelos matemáticos avançados aplicados a problemas práticos, evidenciando a diversidade e a riqueza dos desafios contemporâneos enfrentados por pesquisadores nas Ciências Exatas e da Terra.

O primeiro artigo, *Feições Erosivas em Vargem Alta (Espírito Santo, Brasil)*, trata das dinâmicas de erosão no município de Vargem Alta, com um olhar atento aos processos naturais e suas consequências para o meio ambiente local. Em seguida, *Análise de Estabilidade de Talude no Município de Vargem Alta (ES)* oferece uma análise detalhada sobre a estabilidade de taludes e suas implicações para a segurança das áreas urbanas e rurais afetadas.

No artigo *Contribuição para o Zoneamento de Risco de Inundações Urbanas no Município de Lichinga, Província de Niassa, Moçambique*, o foco se desloca para a aplicação de metodologias para o zoneamento de risco de inundações, um tema de grande importância para o planejamento urbano e a segurança das populações em regiões vulneráveis.

No trabalho *Paleocanais na Plataforma Continental Interna do Rio Grande: Evidências de Variações Eustáticas Durante o Quaternário*, os autores investigam as evidências geológicas de mudanças eustáticas, proporcionando uma compreensão mais profunda dos eventos climáticos e ambientais que marcaram a história do planeta.

No campo da geografia e da agricultura, *Consolidação de Terras Agrícolas (Estudo de Caso Russo)* apresenta um estudo de caso sobre a reorganização da agricultura em uma região da Rússia, discutindo a viabilidade de práticas de consolidação de terras para otimizar o uso da terra e aumentar a produção agrícola.

Seguindo para a física aplicada, o artigo *1D Space-Time Solution of the Species Diffusion Equation with Double Entry Boundary in Spherical Foods* explora soluções matemáticas para a equação de difusão de espécies, com aplicação no setor alimentício, focando na modelagem de processos dentro de esferas alimentícias.

Em seguida, *Modelo Matemático de Difracción en Región de Fresnel Convergente y Divergente de una Lente Esférica* apresenta um modelo matemático inovador para a difração da luz em lentes esféricas, contribuindo para o campo da óptica e suas aplicações.

Por fim, *Caracterización de los Efectos de una Fulguración Solar* discute os impactos de eventos solares extremos, com foco nas implicações para a física espacial e para a proteção de tecnologias modernas sensíveis, como satélites e sistemas de comunicação.

Como é possível observar, este volume é uma contribuição valiosa para o avanço das Ciências Exatas e da Terra, apresentando uma ampla gama de pesquisas que têm o potencial de influenciar práticas em diversas áreas, desde a mitigação de riscos ambientais até o desenvolvimento de novas tecnologias e abordagens inovadoras em várias disciplinas. A variedade de temas e abordagens evidenciam a complexidade dos desafios que os pesquisadores enfrentam atualmente e reforçam a importância da colaboração interdisciplinar para o progresso científico.

Desejo a todos uma proveitosa leitura!

Alireza Mohebi Ashtiani

SUMÁRIO

CAPÍTULO 6

1D SPACE-TIME SOLUTION OF THE SPECIES DIFFUSION EQUATION WITH DOUBLE ENTRY BOUNDARY IN SPHERICAL FOODS[1]

Data de submissão: 11/09/2024
Data de aceite: 27/09/2024

Paula Anabella Giorlando Videla
Universidad Tecnológica Nacional
Facultad Regional Mendoza
Departamento de Ingeniería Química
Mendoza – Argentina
https://orcid.org/0000-0001-5595-9225

Juan Ignacio González Pacheco
Universidad Tecnológica Nacional
Facultad Regional Mendoza
Departamento de Ingeniería Química
Mendoza – Argentina
https://orcid.org/0000-0002-4447-8562

Leonel Nicolás Lisanti
Universidad Tecnológica Nacional
Facultad Regional Mendoza
Departamento de Ingeniería Química
Mendoza – Argentina
https://orcid.org/0000-0002-8623-4953

Mariela Beatriz Maldonado
CONICET
Universidad Tecnológica Nacional
Facultad Regional Mendoza
Departamento de Ingeniería Química
Mendoza – Argentina
https://orcid.org/0000-0002-4188-8005

Carla Rocío Zaragoza
Universidad Tecnológica Nacional
Facultad Regional Mendoza
Departamento de Ingeniería Química
Mendoza – Argentina
https://orcid.org/0000-0001-8262-7744

Ariel Fernando Márquez Agüero
Universidad Tecnológica Nacional
Facultad Regional Mendoza
Departamento de Ingeniería Química
Mendoza – Argentina
https://orcid.org/0000-0003-2330-7905

Oscar Daniel Galvez
Universidad Tecnológica Nacional
Facultad Regional Mendoza
Departamento de Materias Básicas
Mendoza – Argentina
https://orcid.org/0000-0003-4427-3994

[1] The mathematical advancements detailed in this work contribute to the ongoing development of the doctoral thesis of Juan Ignacio González Pacheco, Chemical Engineer. Part of the outcomes derived from the proposed mathematical developments has been featured in the journal *Nature's Scientific Reports*, titled "Diffusion in biological media: a comprehensive numerical-analytical study via surface analysis and diffusivities calculation."

ABSTRACT: The following abstract details our development of a mathematical model to derive the solution of the diffusion equation of chemical species in 1D spherical coordinates. The study concentrates on the proposed boundary conditions for experiments,

aiming to quantify the transport and mechanism by which artificial and natural dyes, such as erythrosine and gardenia red, respectively, diffuse. We used pitted, calibrated, and desulfited cherries (Prunus avium). This work showcases the variation of species concentration concerning the radial position and time while considering third (Robin) and first-type (Dirichlet) boundary conditions, accounting for the cherry's morphology. This development's novelty lies in applying boundary conditions at the flesh-skin-osmotic solution interface, suggesting a double diffusion boundary of substances and introducing a method to calculate effective diffusivities. The methodology employed assumes, as a first approximation, a homogeneous and isotropic flesh with a unidirectional diffusion process, displaying zenithal and azimuthal flow symmetry. Dirichlet conditions were utilised to model a sphere with a hollow spherical centre. Moreover, we discussed the potential inclusion of convective conditions for future work during tests at low stirring speeds (<100 rpm) of the sweetener solution. As a result, a method is introduced to calculate effective diffusivities and concentration profiles in foods with hollow spherical geometry, assuming purely diffusive transport and no external resistance to mass transfer. The proposed condition (Dirichlet) is particularly suitable at high stirring frequencies (220 rpm), with the effective diffusivity being the sole variable to be determined. This study enables a deeper understanding of the transport of chemical species in hollow spherical foods, offering insights into the transport process and laying the groundwork for future research on phenomena with external convective resistance.
KEYWORDS: Mathematical model. Mass diffusion. Boundary conditions. Hollow spherical foods. Effective diffusivity.

SOLUCIÓN ESPACIO-TEMPORAL 1D DE LA ECUACIÓN DE DIFUSIÓN DE ESPECIES CON DOBLE FRONTERA DE INGRESO EN ALIMENTOS ESFÉRICOS

RESUMEN: En el presente trabajo presentamos el desarrollo de un modelo matemático para determinar la solución de la ecuación de difusión de especies químicas en coordenadas esféricas 1D, centrándonos en las condiciones de contorno propuestas para experimentos realizados y cuantificar el transporte y mecanismo en que difunden colorantes artificiales y naturales, como eritrosina y rojo gardenia respectivamente. Los ensayos se realizaron con cerezas (*Prunus avium*) descarozadas, calibradas y desulfitadas. Mostramos la variación de la concentración de especies en función de la posición radial y el tiempo, considerando condiciones de frontera de tercer tipo (Robin) y primer tipo (Dirichlet) teniendo en cuenta la morfología de la cereza. La innovación en el desarrollo radica en la aplicación de condiciones de contorno en la interfaz pulpa-piel-solución osmótica, planteando una doble frontera de ingreso de substancias y la introducción de un método para calcular difusividades efectivas. La metodología empleada supone, como primera aproximación, que la pulpa es homogénea e isótropa, con un proceso de difusión unidireccional, que exhibe simetría de flujo cenital y azimutal. Las condiciones de Dirichlet se utilizaron para modelar una esfera con centro esférico hueco. Además, discutimos la posibilidad de incluir condiciones convectivas para futuros trabajos para ensayos realizados a bajas velocidades de agitación (<100rpm) de la solución edulcorante. Como resultados, se introduce un método para calcular difusividades efectivas y perfiles de concentración en alimentos con geometría esférica hueca, asumiendo transporte puramente difusivo y sin resistencia externa

a la transferencia de masa. La condición propuesta (Dirichlet) resulta ser adecuada particularmente a altas frecuencias de agitación (220 rpm), siendo la difusividad efectiva la única variable a determinar. Este trabajo contribuye a la comprensión del transporte de especies químicas en alimentos esféricos huecos, ofreciendo conocimientos sobre el proceso de transporte y preparando el escenario para futuras investigaciones sobre fenómenos con resistencia convectiva externa.
PALABRAS CLAVE: Modelo matemático. Difusión de masa. Condiciones de contorno. Alimentos esféricos huecos. Difusividad efectiva.

1 INTRODUCTION

Mass diffusive phenomenon, the ubiquitous process driving molecules from high to low concentration, underpins a vast array of food processing and preservation techniques. Understanding its intricate movement within complex food matrices is paramount for optimising process efficiency, ensuring product quality, and extending shelf-life (Junqueira et al., 2021; Khubber et al., 2020; Mugi & Chandramohan, 2021). Mathematical modelling provides a powerful lens through which we can move beyond empirical observations and delve into the quantitative realm of mass transfer phenomena, deciphering the mechanisms governing diffusion in food (M. B. Maldonado et al., 2008; Pereira et al., 2023).

This chapter explores the interplay between diffusion and food engineering, focusing on how a mathematical model, often rooted in Fick's laws, can predict and analyse the movement of substances within food systems. These models provide a theoretical framework for quantifying the rate of mass transfer, enabling us to anticipate and control the impact of processing conditions on the final product (González Pacheco & Maldonado, 2024).

Over the years, a rich tapestry of mathematical models has been woven to capture the nuances of diffusion phenomena. From the elegant simplicity of Fick's laws (González-Pérez et al., 2022; Kian-Pour, 2023; Knee, 2019; Sayago, 2021), which describes diffusion as a gradient-driven process, to more sophisticated approaches that account for heterogeneity, concentration-dependent diffusion, and multicomponent interactions (Bordin et al., 2019; Jamali et al., 2020), these models provide a theoretical framework for understanding how molecules disperse in space and time.

Central to this framework is the concept of effective diffusivity, a measure of how readily molecules navigate the tortuous pathways within a given food matrix. Accurately determining this parameter is crucial for predicting the spatial and temporal distribution of solutes (R. C. da Silva et al., 2022; de Lima Ferreira et al., 2024), water activity, and essential for various food processing and preservation operations, including drying (Macedo et

al., 2022), osmotic dehydration (Meena et al., 2022; Sulistyawati et al., 2020), extraction (Janowicz et al., 2021), packaging (Oladzadabbasabadi et al., 2022), and other key factors influencing food quality and stability (Bae et al., 2020; Pandiselvam et al., 2021). This chapter explores analytical and numerical approaches for determining effective diffusivity (Pinheiro & Castro, 2023; Salehi et al., 2022, 2023), highlighting the strengths and limitations of each method in relation to specific food systems and processing conditions.

The applications of diffusion modelling in food engineering are wide-ranging and significant, encompassing activities such as optimising osmotic dehydration to enhance water removal while maintaining food quality (Brito et al., 2023; Calín-Sánchez et al., 2020; Junqueira et al., 2021), predicting pigment migration for visually appealing products (González Pacheco & Maldonado, 2024; M. Maldonado & González Pacheco, 2022), maximising extraction yields of valuable compounds (Zecchi & Gerla, 2020), and developing effective preservation strategies through an understanding of preservative and spoilage agent transport. Through the utilisation of a quantitative approach, we endeavour to analyse the complexities of diffusion with the objective of establishing an understanding of the governing principles of mass transfer in 1D food systems. This serves as a preliminary stage prior to the advancement to 2D and 3D models. This endeavour ultimately aims to facilitate control, and innovation in the production of safer, higher-quality, and more sustainable food products.

2 MATERIALS AND METHODS

2.1 MATERIALS

A 10-kilogram batch of Prunus avium cultivar Bing was acquired from Luján de Cuyo, Mayor Drummond, Mendoza, Argentina (coordinates in decimal degrees: -33.00443364309908; -68.86583423899584). The materials used in the study included Lactitol powder (DuPont Corporation, Wilmington, Delaware, USA), Maltitol powder (Shandong Lujian Biological Technology Co. Ltd, China), Xylitol powder (Shandong Lujian Biological Technology Co. Ltd, China), as well as Erythrosine powder dye (Macsen Labs, N.K Agrawal Group, India) and Red Gardenia powder dye (Omya Inc., Cincinnati, Ohio, USA).

2.2 METHODS

2.2.1 Processing and Impregnation

The cherries were carefully prepared by calibrating them to a size of 27 mm, pitting, and desulphiting them (sulphur anhydride at 1500 ppm) through immersion in

tap water baths at room temperature for 24 hours, with water renewal every 4 hours. The candying process was initiated using a multiple impregnation method, commonly referred to as the “French or Slow Method”. The sweetener solution with a concentration of 25 Bx was first impregnated, followed by a second impregnation with a 35 Bx syrup to avoid plasmolysis and wrinkles in the fruit (González Pacheco & Maldonado, 2024; M. Maldonado & González Pacheco, 2020, 2022). Erythrosine and red gardenia were added at varying concentrations (119, 238 and 357 ppm) to stain the fruits and observe their influence. The solution was maintained at a steady temperature (40, 50 and 60°C) and subjected to constant agitation to ensure homogeneity (220 rpm). The pH of the sweetening solution was regulated to maintain a specific range for desired outcomes. To maintain the pH of the sweetening solution within the desired range, an approach involving the addition of either 0.9 mL of 10% (w/V) citric acid or 0.3 mL of 10% (w/V) NaHCO3 was executed (APHA, 2017). This procedure is instrumental in ensuring the pH remains between 4.2 and 4.8, leading to a controlled precipitation of the pigment within the cellular structure of the cherry. Consequently, this process enhances the fruit’s vibrant and aesthetically pleasing colouration (Azwanida et al., 2015).

2.2.2 Sampling Process

Cherry samples were randomly selected from multiple container zones for analysis. Cross-sections of the samples were acquired, and the luminosity (L), redness or greenness (a*), and blueness or yellowness (b*) (referred to in combination as CIELAB) were measured using a Minolta CR-400 colourimeter with illuminant D65 (natural light). These measurements were taken from specific points (2.63 mm, 5.26 mm, and 10.53 mm on average) from the centre of the cherry to assess colour properties.

2.3 MATHEMATICAL MODELLING

The experimental data underwent mathematical analysis during the colouration, impregnation process, or osmotic dehydration of fruits in sweetened solutions. This process involved fitting the data to a differential equation that governs the intricate molecular diffusion through the solid, porous hollow sphere constituting the cherry matrix.

2.3.1 Theory

2.3.1.1 Molecular diffusion through a porous solid matrix with spatially constant effective diffusivities subjected to variable boundary conditions. Modelled by double diffusion boundaries in a hollow sphere with constant initial conditions

The Bing variety fruit, illustrated in Figure 1, is medium-sized and heart-shaped. While it demonstrates good on-tree resilience, it is susceptible to cracking. This variety belongs to the Picota type, allowing for stemless harvesting and a central pit. This characteristic facilitates the assumption of an approximately spherical model for the diffusion model resolution, with the pit creating a hollow space at the centre.

Figure 1. Bing variety cherries.

Concerning mathematical modelling for species transfer, we have employed the Reynolds Transport Theorem (RTT) equation. Assuming a constant total molar concentration for the mixture and independent diffusion coefficients with respect to spatial coordinates, we can simplify and express the equation (1) in its tensor form (Bird et al., 2006):

$$\frac{\partial C_i}{\partial t} + (\bar{v}^*.\nabla C_i) = \mathcal{D}_{ij}\nabla^2 C_i + R_i - \frac{C_i}{C}\left(R_i + R_j\right) \qquad (1)$$

The molar concentration of species in the mixture is denoted as C_i, while D_{ij} represents the effective diffusivity for a binary system. The local average molar velocity of the mixture is represented by $\bar{v}^*$and the species unit volume production rate due to chemical reactions is denoted by R_i or R_j. The variable t represents time.

Hence, the one-dimensional, non-dimensional diffusion equation with constant effective diffusivities in the flesh (D_F) and skin (D_S), considering only the molecular diffusion of dyes as a transport mechanism within the fruit and without accounting for

the generation of substances through chemical reactions, can be expressed as a partial differential equation, denoted as equation (2) (Carslaw & Jaeger, 1959; Crank, 1979; Hahn & Özişik, 2012):

$$\frac{\partial C}{\partial \Theta} = \frac{2}{R}\frac{\partial C}{\partial R} + \frac{\partial^2 C}{\partial R^2} \qquad (2)$$

Where

$$\Theta = \frac{D_{ij}\, t}{{r_o}^2};\ R = \frac{r}{r_0};\ C = \frac{C_{(t)} - C_s}{C_i - C_s}$$

Consider that theta, Θ, is a non-dimensional time, R is a non-dimensional radius, C represents a non-dimensional concentration, $C_{(t)}$ denotes the dye concentration within the cherry flesh as time progresses, C_s represents the dye concentration in the cherry skin in contact with the sweetening solution (Zuritz & Maldonado, 2004), and C_i denotes the dye concentration within the cherry flesh at the beginning of the experiment (Figure 2).

Figure 2. Representation of the staining trials conducted with erythrosine and red gardenia at 119, 238, and 357 ppm and at 40, 50, and 60°C. Visualisation of the experimental conditions to provide a rationale for the boundary conditions defined in the mathematical framework. Created in BioRender. González Pacheco, J. (2024) BioRender.com/t24d848.

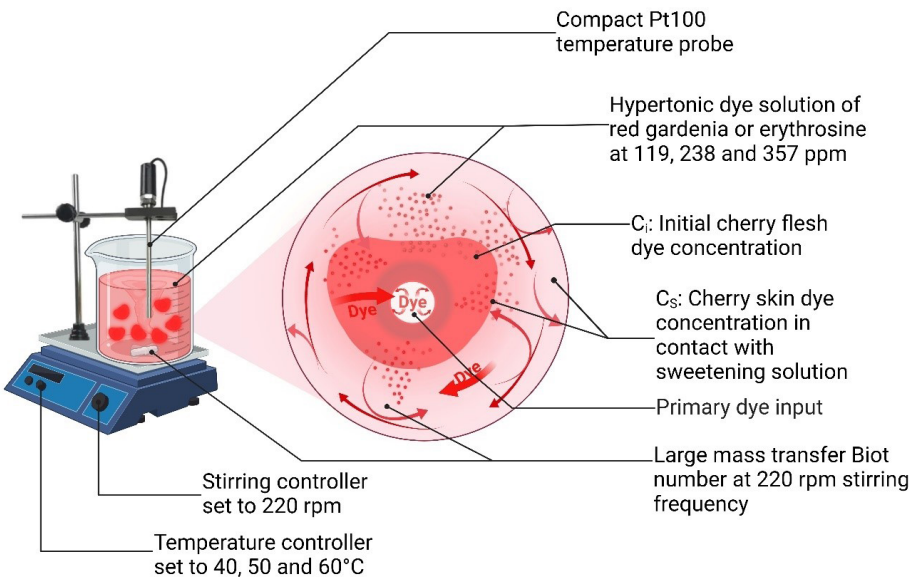

The physical properties of cherry flesh were initially approximated as homogeneous and isotropic, assuming a unidirectional radial diffusion process. The high agitation of the sweetening solution surrounding the inner and outer surfaces (220 rpm) led to the assumption that the concentration in these areas immediately equates

to the concentration of the liquid (large mass Biot number). Additionally, the thickness of the epidermis was considered much smaller than the radii of the inner and outer faces, allowing the difference in surface areas to be ignored and the thickness to be assumed as $r_s - r_0$. Moreover, it was deemed appropriate to assume that solute accumulation in the skin, represented by $r_s - r_0$, and consequently the resistance to species transfer, is negligible compared to the flux through the porous surface and the flux itself, which is given by the cherry skin with a thickness of 0.0004 m (Fig. 3).

Furthermore, we postulated that a double diffusion boundary exists at the flesh-skin interface of the fruit, attributed to the primary entry of colourant from the pitted area and an additional incoming flow through the porous matrix skin, which allows the entry of both soluble solids and colourant. This dual penetration phenomenon (Figure 3) will be mathematically modelled by implementing B.C.2, equation (6), a mixed boundary condition.

Figure 3. Visualisation of the primary movement patterns during the colouring, along with the dye penetration at the double diffusion boundary located at the junction between the flesh and the fruit's skin. Created in BioRender. González Pacheco, J. (2024) BioRender.com/t24d848.

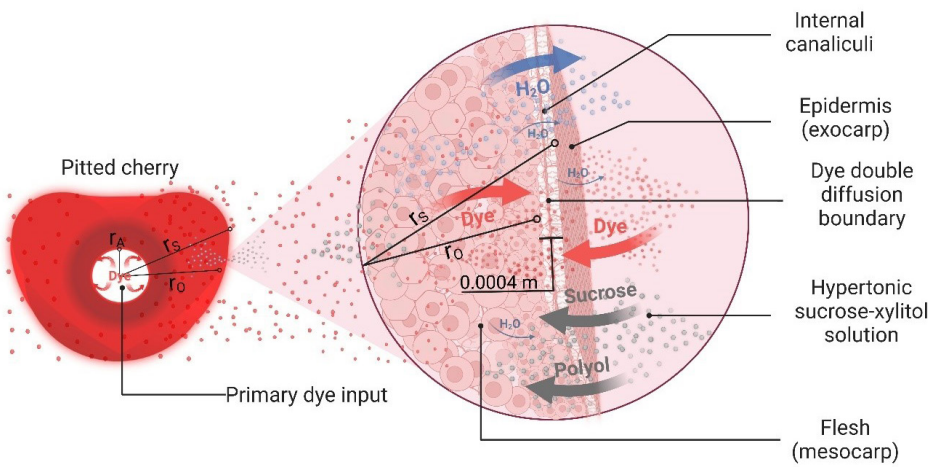

2.3.2 CALCULATION

An alternative form of equation (2) was derived by utilising a fitting process for the redness parameter a*, employing the least squares method with a linear approach. The objective of this process was to establish a relationship between the concentration of erythrosine or red gardenia dye, as described in equation (3), and the experimental data. This facilitated the derivation of a refined version of equation (2). This correlation provides an alternative method for presenting the transport of 1D species and their properties in general by introducing the redness parameter, a*.

$$\frac{\partial a^*}{\partial \Theta} = \frac{2}{R}\frac{\partial a^*}{\partial R} + \frac{\partial^2 a^*}{\partial R^2} \quad (3)$$

Subjected by the following dimensionless initial and boundary conditions:

$$I.C.: At\ \Theta = 0 \qquad a^* = \frac{{a_i}^* - {a_s}^*}{{a_i}^* - {a_s}^*} = 1 \qquad at \quad A \leq R \leq 1 \quad (4)$$

$$B.C.1: At\ \Theta > 0 \qquad a^* = \frac{{a_s}^* - {a_s}^*}{{a_i}^* - {a_s}^*} = 0 \qquad at \qquad R = A \quad (5)$$

$$B.C.2: At\ \Theta > 0 \qquad \frac{\partial a^*}{\partial R} + \frac{D_S}{D_F}\left(\frac{r_0}{r_s - r_0}\right)a^* = 0 \qquad at \qquad R = 1 \quad (6)$$

Where

$$\Theta = \frac{\mathcal{D}_{ij}\ t}{{r_o}^2};\ R = \frac{r}{r_0};\ A = \frac{r_A}{r_0};\ a^* = \frac{{a_{(t)}}^* - {a_s}^*}{{a_i}^* - {a_s}^*}$$

In the context of the experiment, the dimensionless radius “A” is calculated as the ratio between and . Additionally, the variables $a_{(t)}*$, a_s* and a_i* are utilised to quantify the redness of the cherry flesh during the experiment. $a_{(t)}*$ denotes the evolving redness of the cherry flesh over time, while a_s* signifies the redness of the cherry skin upon contact with the sweetening solution. Lastly, a_i* signifies the initial redness of the cherry flesh at the outset of the experiment.

On the other hand, we will begin by addressing the second boundary condition, B.C.2, equation (6), which is non-homogeneous. Due to this characteristic, the separation of variables method will be employed.

The solution to the primary non-homogeneous problem takes the following form:

$${a^*}_{(R,\Theta)} = \sum_n A_{n(\Theta)}\Phi_{n(R)} \quad (7)$$

According to the orthogonality of $\Phi_{n(R)}$:

$$\int_A^1 {a^*}_{(R,\Theta)} W_{(R)}\ \Phi_{m(R)} dR = \sum_n A_{n(\Theta)} \int_A^1 W_{(R)}\Phi_{m(R)}\ \Phi_{n(R)} dR \quad (8)$$

Further:

$$\int_A^1 a^*{}_{(R,\Theta)} W_{(R)}\, \phi_{m(R)} dR = bA_{m(\Theta)} \tag{9}$$

And:

$$A_{m(\Theta)} = \frac{1}{b}\int_A^1 a^*{}_{(R,\Theta)} W_{(R)}\, \phi_{m(R)} dR \tag{10}$$

The addition of the function $W_{(R)}$ introduces orthogonality, ensuring that $\phi_{m(R)}$ and $\phi_{n(R)}$ are orthogonal to $W_{(R)}$ in (A, 1).

$$\int_A^1 W_{(R)} \phi_{m(R)}\, \phi_{n(R)} dR = \begin{cases} 0 & for\ m \neq n \\ b & for\ m = n \end{cases}$$

Now, turning our attention to a homogeneous problem ($a^* = u$):

$$\frac{\partial u}{\partial \Theta} = \frac{2}{R}\frac{\partial u}{\partial R} + \frac{\partial^2 u}{\partial R^2} \tag{11}$$

$$I.C.: \quad At\ \Theta = 0 \qquad u = 1 \qquad at \qquad A \leq R \leq 1 \tag{11.1}$$

$$B.C.1: At\ \Theta > 0 \qquad u = 0 \qquad at \qquad R = A \tag{11.2}$$

$$B.C.2: At\ \Theta > 0 \qquad \frac{\partial u}{\partial R} = 0 \qquad at \qquad R = 1 \tag{11.3}$$

We present a solution to the homogeneous equation (11). The subscripts on the functions denote the number of derivatives with respect to the corresponding variable.

$$u_{(R,\theta)} = \Re_{(R)} \check{O}_{(\theta)} \tag{12}$$

$$\ddot{\Re}_{(R)} \check{O}_{(\theta)} + \frac{2}{R} \check{O}_{(\theta)} \dot{\Re}_{(R)} = \Re_{(R)} \dot{\check{O}}_{(\theta)} \tag{12.1}$$

$$\frac{1}{\Re}\frac{d^2\Re}{d\Re^2} + \frac{2}{\Re R}\frac{d\Re}{dR} = \frac{1}{\check{O}}\frac{d\check{O}}{d\theta} = -\lambda^2 \tag{12.2}$$

In the given scenario, a positive constant is symbolised as λ^2. To ensure that the solution approaches zero as time, Θ, increases, a negative constant, denoted as $-\lambda^2$, is deliberately selected. Opting for a positive constant or zero instead would lead to a solution that grows indefinitely as Θ progresses. From a mathematical perspective, this

selection would not correspond to the physical phenomenon that the solution must eventually approach finite boundary conditions.

Then:

$$\begin{cases} \ddot{\Re}R^2 + 2R\dot{\Re} + \lambda^2 R^2 \Re = 0 \\ \dot{\Ö} + \lambda^2 \Ö = 0 \end{cases}$$

Whose solutions are:

$$\Re_{(\lambda_n R)} = R^{-\frac{1}{2}}\left[C_1 J_{\frac{1}{2}(\lambda_n R)} + C_2 Y_{\frac{1}{2}(\lambda_n R)}\right] \tag{13}$$

$$\Ö_{\lambda_n} = C_3 e^{-{\lambda_n}^2 \theta} \tag{14}$$

We can consider $Y_{\frac{1}{2}(\lambda_n R)}$ as a Neumann function or Bessel function of the second kind by proposal, leading to:

$$\Re_{(\lambda_n R)} = R^{-\frac{1}{2}}\left[C_1 J_{\frac{1}{2}(\lambda_n R)} - C_2 J_{-\frac{1}{2}(\lambda_n R)}\right] \tag{15}$$

Bessel functions of the first kind can be explicitly expressed as follows:

$$J_{n(\lambda R)} = (\lambda R)^n \sum_{m=0}^{\infty} \frac{(-1)^m (\lambda R)^{2m}}{2^{2m+n}\, m!\ \Gamma(n+m+1)} \tag{16}$$

Then:

$$J_{\frac{1}{2}(\lambda R)} = \sqrt{\frac{2}{\pi \lambda R}} \sin \lambda R \ \ and \ \ J_{-\frac{1}{2}(\lambda R)} = \sqrt{\frac{2}{\pi \lambda R}} \cos \lambda R \tag{17}$$

By replacing equations (17) in equation (15):

$$\Re_{(\lambda_n R)} = R^{-\frac{1}{2}}\left[C_1 \sqrt{\frac{2}{\pi \lambda_n R}} \sin \lambda_n R - C_2 \sqrt{\frac{2}{\pi \lambda_n R}} \cos \lambda_n R\right] = \frac{1}{R}\left[C_1 \sqrt{\frac{2}{\pi \lambda_n}} \sin \lambda_n R - C_2 \sqrt{\frac{2}{\pi \lambda_n}} \cos \lambda_n R\right] \tag{18}$$

Finally:

$$u_{(R,\theta)} = \frac{1}{R}\left[\mathbb{C}_1 \sqrt{\frac{2}{\pi \lambda_n}} \sin \lambda_n R - \mathbb{C}_2 \sqrt{\frac{2}{\pi \lambda_n}} \cos \lambda_n R\right] e^{-{\lambda_n}^2 \theta} \tag{19}$$

Where $\mathbb{C}_1 = C_1C_3$ and $\mathbb{C}_2 = C_2C_3$.

We apply the B.C.1, equation (11.2) in expression (19):

$$u_{(A,\theta)} = 0 = \frac{1}{A}\left[\mathbb{C}_1\sqrt{\frac{2}{\pi\lambda_n}}\sin\lambda_n A - \mathbb{C}_2\sqrt{\frac{2}{\pi\lambda_n}}\cos\lambda_n A\right]e^{-{\lambda_n}^2\theta}$$

Hence: $-\frac{\mathbb{C}_2}{\mathbb{C}_1} = -\frac{\sin\lambda_n A}{\cos\lambda_n A} = -\tan\lambda_n A$ (20)

When we differentiate equation (28) with respect to R at R=1 using the B.C.2, we obtain the following result

$$\left.\frac{\partial u}{\partial R}\right|_{R=1} = 0 = e^{-{\lambda_n}^2\theta}\sqrt{\frac{2}{\pi\lambda_n}}[\mathbb{C}_1(\lambda_n\cos\lambda_n - \sin\lambda_n) + \mathbb{C}_2(\lambda_n\sin\lambda_n + \cos\lambda_n)]$$

Hence:

$$-\frac{\mathbb{C}_2}{\mathbb{C}_1} = \frac{(\lambda_n\cos\lambda_n - \sin\lambda_n)}{(\lambda_n\sin\lambda_n + \cos\lambda_n)} \quad (21)$$

Further:

$$-\frac{\mathbb{C}_2}{\mathbb{C}_1} = \frac{(\lambda_n\cos\lambda_n - \sin\lambda_n)}{(\lambda_n\sin\lambda_n + \cos\lambda_n)} = -\frac{\sin\lambda_n A}{\cos\lambda_n A} \quad (22)$$

Now, we can derive the equation of the homogeneous problem:

$$\sin\lambda_n\,(\lambda_n\sin\lambda_n A - \cos\lambda_n A) + \cos\lambda_n\,(\sin\lambda_n A + \lambda_n\cos\lambda_n A) = 0 \quad (23)$$

Equation (23) allows the calculation of the eigenvalues λ_n. Then:

$$u_{(R,\theta)} = \Re_{(\lambda_n R)}\breve{\mathrm{O}}_{(\theta)} = \frac{1}{R}\left[\mathbb{C}_1\sqrt{\frac{2}{\pi\lambda_n}}\sin\lambda_n R - \mathbb{C}_2\sqrt{\frac{2}{\pi\lambda_n}}\cos\lambda_n R\right]e^{-{\lambda_n}^2\theta}$$

$$= \frac{\mathbb{C}_1}{R}\sqrt{\frac{2}{\pi\lambda_n}}\left[\sin\lambda_n R - \frac{\mathbb{C}_2}{\mathbb{C}_1}\cos\lambda_n R\right]e^{-{\lambda_n}^2\theta}$$

$$= A_{n(\Theta)}S_{(\lambda_n R)} \quad (24)$$

There are clear similarities between equation (24), which represents the solution of the homogeneous problem, and equation (7), which represents the solution of the non-homogeneous problem.

$$S_{(\lambda_n R)} = \frac{1}{R}\sqrt{\frac{2}{\pi\lambda_n}}\left[\sin\lambda_n R - \frac{C_2}{C_1}\cos\lambda_n R\right]$$

$$= \frac{1}{R}\sqrt{\frac{2}{\pi\lambda_n}}\left[\sin\lambda_n R + \frac{(\lambda_n\cos\lambda_n - \sin\lambda_n)}{(\lambda_n\sin\lambda_n + \cos\lambda_n)}\cos\lambda_n R\right] \cong \Phi_{n(R)} \qquad (25)$$

Whilst $A_{n(\Theta)}$ will be $A_{n(\Theta)} = \mathbb{C}_1 e^{-\lambda_n{}^2\Theta}$, to be determined from the non-homogeneous solution. If we multiply equation (7) by $\Phi_{n(R)}$ and $w(R) = R^2$, and integrating from R = A to R = 1:

$$\int_A^1 a^*{}_{(R,\Theta)} R^2\,\Phi_{n(R)}\,dR = \sum_n^\infty A_{n(\Theta)}\int_A^1 R^2\,\Phi_{n(R)}{}^2\,dR, \text{ solving for } A_{m(\Theta)}:$$

$$A_{m(\Theta)} = \frac{\int_A^1 a^*{}_{(R,\Theta)} W_{(R)}\,\Phi_{m(R)}\,dR}{\int_A^1 R^2\,\Phi_{m(R)}{}^2\,dR} = \frac{1}{b}\int_A^1 a^*{}_{(R,\Theta)} R^2\,\Phi_{m(R)}\,dR \qquad (26)$$

Where: $$b = \int_A^1 R^2\,\Phi_{m(R)}{}^2\,dR \qquad (27)$$

The subsequent step involves establishing an ordinary differential equation for $A_{m(\Theta)}$. We proceed by deriving equation (26) with respect to the dimensionless time Θ. Notably, as Θ does not influence the integration limits, the following equation is derived:

$$\frac{dA_{m(\Theta)}}{d\Theta} = \frac{1}{b}\int_a^1 \left(\frac{\partial^2 a^*}{\partial R^2}\right) R^2\,\Phi_{m(R)}\,dR + \frac{2}{b}\int_a^1 \left(\frac{\partial a^*}{\partial R}\right) R\,\Phi_{m(R)}\,dR \qquad (28)$$

Upon substituting equation (25) into equation (27) and solving for "b", this can be determined as:

$$b = \frac{1}{\pi\lambda_n}\left\{\left[(1-A) + \frac{\sin(2\lambda_n A) - \sin(2\lambda_n)}{2\lambda_n}\right] + \frac{2}{\lambda_n}\frac{[\lambda_n\cos(\lambda_n) - \sin(\lambda_n)]}{[\lambda_n\sin(\lambda_n) + \cos(\lambda_n)]}[\sin^2(\lambda_n) - \sin^2(\lambda_n A)] + \frac{[\lambda_n\cos(\lambda_n) - \sin(\lambda_n)]^2}{[\lambda_n\sin(\lambda_n) + \cos(\lambda_n)]^2}\left[(1-A) - \frac{\sin(2\lambda_n A) - \sin(2\lambda_n)}{2\lambda_n}\right]\right\} \qquad (30)$$

If equation (25) is substituted into equation (28), the resultant outcome will be as follows:

$$\frac{dA_{m(\theta)}}{d\Theta} = \frac{1}{b}\sqrt{\frac{2}{\pi\lambda_n}}\int_A^1 \left(\frac{\partial^2 a^*}{\partial R^2}\right) R\left[\sin(\lambda_n R) + \frac{[\lambda_n \cos(\lambda_n) - \sin(\lambda_n)]}{[\lambda_n \sin(\lambda_n) + \cos(\lambda_n)]}\cos(\lambda_n R)\right] dR$$
$$+ \frac{2}{b}\sqrt{\frac{2}{\pi\lambda_n}}\int_A^1 \left(\frac{\partial a^*}{\partial R}\right)\left[\sin(\lambda_n R) + \frac{[\lambda_n \cos(\lambda_n) - \sin(\lambda_n)]}{[\lambda_n \sin(\lambda_n) + \cos(\lambda_n)]}\cos(\lambda_n R)\right] dR \quad (31)$$

We will now proceed with solving the ordinary differential equation for $A_{m(\theta)}$:

$$\frac{dA_{m(\theta)}}{d\Theta} = \frac{1}{b}\sqrt{\frac{2}{\pi\lambda_n}}\int_A^1 \left(\frac{\partial a^*}{\partial R}\right)\left\{\left[\sin(\lambda_n R) + \frac{[\lambda_n \cos(\lambda_n) - \sin(\lambda_n)]}{[\lambda_n \sin(\lambda_n) + \cos(\lambda_n)]}\cos(\lambda_n R)\right]\right.$$
$$\left. - R\lambda_n\left[\cos(\lambda_n R) - \frac{[\lambda_n \cos(\lambda_n) - \sin(\lambda_n)]}{[\lambda_n \sin(\lambda_n) + \cos(\lambda_n)]}\sin(\lambda_n R)\right]\right\} dR$$
$$= \frac{1}{b}\sqrt{\frac{2}{\pi\lambda_n}}\left|a^*_{(R,\theta)}\left[\left[\sin(\lambda_n R) + \frac{[\lambda_n \cos(\lambda_n) - \sin(\lambda_n)]}{[\lambda_n \sin(\lambda_n) + \cos(\lambda_n)]}\cos(\lambda_n R)\right]\right.\right.$$
$$\left.\left. - R\lambda_n\left[\cos(\lambda_n R) - \frac{[\lambda_n \cos(\lambda_n) - \sin(\lambda_n)]}{[\lambda_n \sin(\lambda_n) + \cos(\lambda_n)]}\sin(\lambda_n R)\right]\right]\right|_A^1$$
$$- \frac{1}{b}\sqrt{\frac{2}{\pi\lambda_n}}\int_A^1 a^*_{(R,\theta)}{\lambda_n}^2 R\left[\sin(\lambda_n R)\right.$$
$$\left. + \frac{[\lambda_n \cos(\lambda_n) - \sin(\lambda_n)]}{[\lambda_n \sin(\lambda_n) + \cos(\lambda_n)]}\cos(\lambda_n R)\right] dR \quad (32)$$

It is noted that by multiplying and dividing the integral of equation (32) by R and rearranging the terms, we can derive the expression for $A_{m(\theta)}$ multiplied by ${\lambda_n}^2$.

$$\frac{dA_{m(\theta)}}{d\Theta} = \frac{1}{b}\sqrt{\frac{2}{\pi\lambda_n}}\int_a^1 \left(\frac{\partial a^*}{\partial R}\right)\left\{\left[\sin(\lambda_n R) + \frac{[\lambda_n \cos(\lambda_n) - \sin(\lambda_n)]}{[\lambda_n \sin(\lambda_n) + \cos(\lambda_n)]}\cos(\lambda_n R)\right]\right.$$
$$\left. - R\lambda_n\left[\cos(\lambda_n R) - \frac{[\lambda_n \cos(\lambda_n) - \sin(\lambda_n)]}{[\lambda_n \sin(\lambda_n) + \cos(\lambda_n)]}\sin(\lambda_n R)\right]\right\} dR$$
$$= \frac{1}{b}\sqrt{\frac{2}{\pi\lambda_n}}\left|a^*_{(R,\theta)}\left[\left[\sin(\lambda_n R) + \frac{[\lambda_n \cos(\lambda_n) - \sin(\lambda_n)]}{[\lambda_n \sin(\lambda_n) + \cos(\lambda_n)]}\cos(\lambda_n R)\right]\right.\right.$$
$$\left.\left. - R\lambda_n\left[\cos(\lambda_n R) - \frac{[\lambda_n \cos(\lambda_n) - \sin(\lambda_n)]}{[\lambda_n \sin(\lambda_n) + \cos(\lambda_n)]}\sin(\lambda_n R)\right]\right]\right|_a^1$$
$$- {\lambda_n}^2 A_{m(\theta)} \quad (33)$$

To address equation (33), we can resolve it by utilising the equalities outlined in equation (22).

✓ At R=1:

$$a^*_{(R,\Theta)}\left\{\frac{\sin\lambda\,(\lambda\sin\lambda A-\cos\lambda A)+\cos\lambda\,(\sin\lambda A+\lambda\cos\lambda A)}{\cos\lambda A}\right\}=0 \tag{34}$$

✓ At R=A:

$$a^*_{(R,\Theta)}\left\{\sin\lambda R+\left(\frac{\lambda_n\cos\lambda_n-\sin\lambda_n}{\lambda_n\sin\lambda_n+\cos\lambda_n}\right)\cos\lambda_n R-\lambda_n R\left[\cos\lambda_n R-\left(\frac{\lambda_n\cos\lambda_n-\sin\lambda_n}{\lambda_n\sin\lambda_n+\cos\lambda_n}\right)\sin\lambda_n R\right]\right\}\Bigg|_A^0=0 \tag{35}$$

Hence:

$$\frac{dA_{m(\Theta)}}{d\Theta}+{\lambda_n}^2A_{m(\Theta)}=\frac{1}{b}\sqrt{\frac{2}{\pi\lambda_n}}\left\{\left(\frac{\partial a^*}{\partial R}\right)_{R=1}\left[\sin\lambda_n+\left(\frac{\lambda_n\cos\lambda_n-\sin\lambda_n}{\lambda_n\sin\lambda_n+\cos\lambda_n}\right)\cos\lambda_n\right]\right\} \tag{36}$$

Furthermore, by B.C.2, equation (6), we know that $\left.\frac{\partial a^*}{\partial R}\right|_{R=1}^{0}=-\frac{D_S}{D_F}\left(\frac{r_0}{r_s-r_0}\right)a^*$. Replacing equation (6) in (36), we further define: $W=\frac{1}{b}\sqrt{\frac{2}{\pi\lambda_n}}\left\{\frac{D_S}{D_F}\left(\frac{r_0}{r_s-r_0}\right)\left[\sin\lambda_n+\left(\frac{\lambda_n\cos\lambda_n-\sin\lambda_n}{\lambda_n\sin\lambda_n+\cos\lambda_n}\right)\cos\lambda_n\right]\right\}$. Furthermore, commencing from the definition of a*, it can be expressed as: $a^*=\frac{a^*_{(t)}-a^*_s}{a^*_i-a^*_s}$. In this definition, both a^*_S and a^*_i, remain constant and do not vary according to R or Θ. Whereas $a^*_{(t)}$ at R=1, Since R is fixed, it will only depend on time. Consequently, it is plausible to consider $a^*=\xi_{(\Theta)}$. Then:

$$\frac{dA_{m(\Theta)}}{d\Theta}+{\lambda_n}^2A_{m(\Theta)}=-W\xi_{(\Theta)} \tag{37}$$

Equation (37) represents the ordinary differential equation for $A_{m(\theta)}$, providing the solution needed to solve the final equation (7). Employing $e^{\lambda^2\Theta}$ as the integration factor, and using the initial condition $a^*_{(R,0)}=1$, considering the definition in equation (26):

$$A_{m(\Theta)}=\left(\frac{1}{b}\int_A^1 R^2\,\Phi_{m(R)}dR-W\int_0^\Theta \xi_{(\Theta)}e^{{\lambda_n}^2\Theta}d\Theta\right)e^{-{\lambda_n}^2\Theta} \tag{38}$$

3 RESULTS AND DISCUSSION

In order to establish a relationship for $\xi_{(\Theta)}$, we can refer to equation (14), which provides the proposed temporal solution for the homogeneous problem: $\breve{O}_{\lambda n}=C_3e^{-{\lambda_n}^2\Theta}$. This expression represents a constant multiplied by an exponential function that decreases with time. It is well-established, both analytically and experimentally, that the function $\xi_{(\Theta)}$ follows an exponential decay over time, akin to the Arrhenius equation.

Therefore, we propose a model as follows: $\xi_{(\Theta)}=\mathbb{C}_0e^{-\mathbb{C}_5\Theta}$ (39)

Upon substituting equation (39) into the second integral of equation (38) and solving it:

$$A_{m(\theta)} = \left(\frac{1}{b}\int_A^1 R^2\,\Phi_{m(R)}dR - \frac{W\mathbb{C}_0}{{\lambda_n}^2 - \mathbb{C}_5}\left[e^{({\lambda_n}^2-\mathbb{C}_5)\theta} - 1\right]\right) e^{-{\lambda_n}^2\theta} \tag{40}$$

Upon substitution of equation (40) into equation (7):

$$a^*_{(R,\theta)} = \sum_{n=1}^{\infty}\left(\frac{1}{b}\int_A^1 R^2\,\Phi_{n(R)}dR - \frac{W\mathbb{C}_0}{{\lambda_n}^2 - \mathbb{C}_5}\left[e^{({\lambda_n}^2-\mathbb{C}_5)\theta} - 1\right]\right) e^{-{\lambda_n}^2\theta}\,\Phi_{n(R)} \tag{41}$$

The average volumetric parameter, denoted as ${a_V}^*{}_{(\Theta)}$ will be determined through integration using the following expression:

$${a_V}^*{}_{(\Theta)} = \frac{3}{(1-A^3)}\int_A^1 a^*_{(R,\Theta)}\,R^2dR \tag{42}$$

Hence, by substituting equation (41) into expression (42), the evolution of the dimensionless volumetric parameter ${a_V}^*{}_{(\Theta)}$ with respect to the dimensionless time Θ can be derived. This analytical representation can be expanded as an infinite series, as detailed in equation (43). It is an adapted form of the original equation initially proposed by Maldonado & González Pacheco (2022) and verified by González Pacheco & Maldonado (2024).

$$\begin{aligned}{a_V}^*{}_{(\Theta)} = \frac{3}{(1-A^3)}\sum_{n=1}^{\infty}\Bigg\{&\frac{1}{b}\left[\int_A^1 R^2\,\Phi_{n(R)}dR\right]^2 \\ &- \frac{W\mathbb{C}_0}{{\lambda_n}^2 - \mathbb{C}_5}\left[e^{({\lambda_n}^2-\mathbb{C}_5)\theta} - 1\right]\int_A^1 R^2\Phi_{n(R)}\,dR\Bigg\}\,e^{-{\lambda_n}^2\theta}\end{aligned} \tag{43}$$

The effective diffusion coefficients and eigenvalues λ_n were determined using an iterative nonlinear regression method in conjunction with *GraphPad PRISM© Software (V9.5.1, MA, USA)*, employing the least squares method. Furthermore, we utilised the minimum chi-square method to assess the model's suitability. When dealing with a large mass transfer Biot number under the given conditions and the specified boundary condition (equation 5), it is important to note that significant truncation errors may occur, especially during the initial stages of the process. It is considered inappropriate to rely on nonlinear regression with a limited number of terms in the series of analytical solutions to obtain precise results for determining effective diffusivity. As a result, the first 220 terms of the analytical solution were incorporated alongside the optimiser (W. P. da Silva et al., 2009, 2018). We will now adopt a function to account for the temporal variation of the volumetric parameter ${a_V}^*{}_{(\Theta)}$:

$$\mathbb{C}_0 = \frac{6}{(1-A^3)}{R_{\lambda_n}}^2 \tag{44}$$

$$\mathbb{C}_5 = {\lambda_n}^{2.0031} \tag{45}$$

Where:

$$R_{\lambda_1} = (B_3C_3) - (D_3E_3) + A\lambda_1(B_3E_3 + D_3C_3) \quad (46)$$

Additionally:

$$B_3 = \frac{\cos(\lambda_n A)}{\lambda_n} \quad (47)$$

$$C_3 = \frac{1}{\lambda_n}[\sin(\lambda_n) - \sin(\lambda_n A)] + [A\cos(\lambda_n A) - \cos(\lambda_n)] \quad (48)$$

$$D_3 = \frac{\sin(\lambda_n A)}{\lambda_n} \quad (49)$$

$$E_3 = \frac{1}{\lambda_n}[\cos(\lambda_n) - \cos(\lambda_n A)] + [\sin(\lambda_n) - A\sin(\lambda_n A)] \quad (50)$$

On the other hand, W. P. da Silva et al. (2018) conducted an investigation using a convective-type boundary condition to simulate pure diffusive transport and convective phenomena. The study emphasised the existence of external resistance to mass transfer at low stirring frequencies (<100 rpm) during the extraction process of anthocyanin dye from jambolan (Syzygium cumini (L.)). Similarly, in our current research, we propose a method for calculating effective diffusivities and concentration profiles (Fig. 4.a.) in cherries (Prunus avium) assuming purely diffusive transport and neglecting external resistance to mass transfer. We also analysed the sensitivity of a* based on the location within the cherry flesh. Our findings revealed a pronounced dye penetration at the periphery, followed by penetration through the centre of the cherry ($p<0.05$). The results indicate a double diffusion boundary at the cherry's flesh-skin interface (Fig. 4.b.). We generated surface graphs to illustrate the evolution of the gardenia red dye concentration, denoted as "redness," as a function of both time and radial distance within the cherries. The presence of a double diffusion boundary at approximately 12 mm is discernible in the visual representation (Fig. 4.c.). The boundary condition advocated in our study (equation 5) is considered appropriate, particularly at a high stirring frequency of 220 rpm, where the principal variable requiring determination is the effective mass diffusivity, given a large Biot (Bi) number. However, we intend to explore convective boundary conditions in future work to clarify the transport mechanism of substances at low stirring velocities.

Figure 4. a-c. Time-dependent fluctuations in the input (in) and output (out) concentrations of red gardenia (RG) dye at 119 ppm and temperature of 40°C. These fluctuations were analysed using the hollow sphere model. Data was fitted to the analytical model using 220 terms of the infinite series. Following adjustments to the concentration values, the determination coefficient (R^2) exceeded 99%, and a minimal chi-square value (χ^2) was achieved (a). Sensitivity of the redness parameter a* to the position inside the cherry (2.63, 5.26, and 10.53 mm measured from the centre). Data are expressed as mean ± SD, two-way ANOVA with Tukey multiple comparisons test, with statistical significance defined as $p < 0.05$ (b). Surface plot depicting the variation of red gardenia dye concentration profile, expressed as redness, as a function of time and radial distance within cherries at 40°C, with a concentration of 119ppm, respectively (c). Figure 4.b. was created in BioRender. González Pacheco, J. (2024) BioRender.com/t24d848.

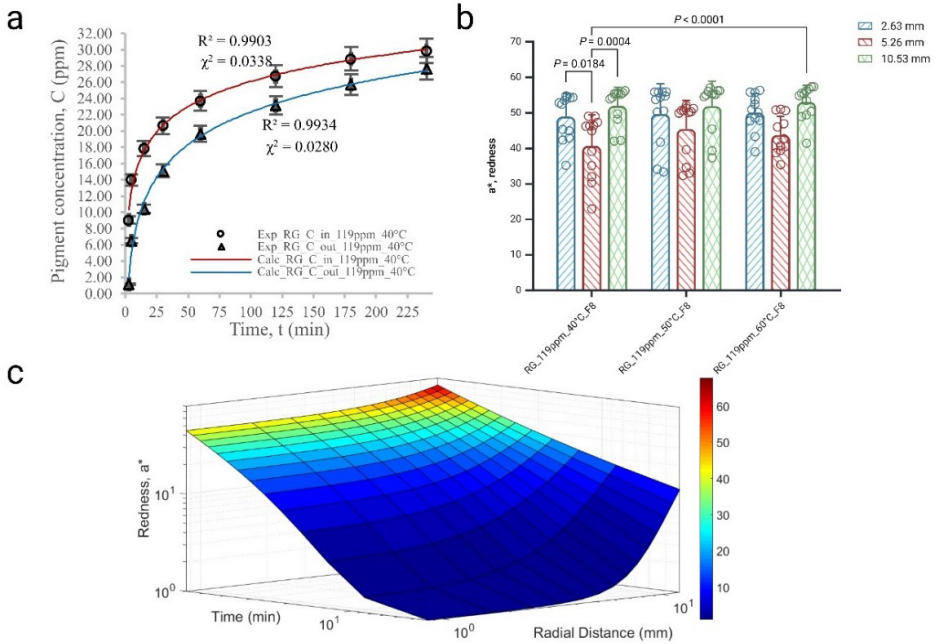

4 CONCLUSIONS

The mathematical model developed in this study provides insights into the diffusion of chemical species in 1D spherical coordinates, particularly focusing on hollow spherical foods. The application of boundary conditions at the interface of the flesh-skin-osmotic solution and the introduction of a method to calculate effective diffusivities represent advancements in the understanding of mass transport phenomena in such food geometries. The findings presented in this work offer knowledge regarding the transport processes in hollow spherical foods and pave the way for future investigations into phenomena involving external convective resistance. The quantitative analysis of species diffusion in this context contributes to the understanding of mass transport in food systems and holds the potential for enhancing food processing and preservation techniques.

REFERENCES

APHA. (2017). **Standard Methods for the Examination of Water and Wastewater**. Federation. Water Environmental American Public Health Association (APHA),Washington, DC, USA. Federation. Washington DC.

AZWANIDA, N. N., HUI, M. S., AFANDI, A., MOHAMED, S., K, Z. A., AYOB, A., RUSLI, N., RASAT, M. S. M., & MOHAMED, M. (2015). Color Stability Evaluation of Pigment Extracted from Hylocereus polyrhizus, Clitorea ternatae and Pandanus amaryllfolius as Cosmetic Colorants and Premarket Survey on Customer Acceptance on Natural Cosmetic Product. **Journal of Tropical Resources and Sustainable Science** (JTRSS), 3(1). https://doi.org/10.47253/jtrss.v3i1.690

BAE, S., CHOI, J. Y., LEE, H. J., KIM, J., & MOON, K. D. (2020). The effect of osmotic dehydration pretreatment with sweeteners on the quality of dried aronia berries. **Korean Journal of Food Preservation**, 27(4). https://doi.org/10.11002/KJFP.2020.27.4.468

BIRD, R. B., STEWART, W. E., & LIGHTFOOT, E. N. (2006). Transport Phenomena. In **Transport Phenomena** (2nd ed.). John Wiley & Sons.

BORDIN, M. S. P., BORSATO, D., CREMASCO, H., GALVAN, D., SILVA, L. R. C., ROMAGNOLI, É. S., & ANGILELLI, K. G. (2019). Mathematical modeling of multicomponent NaCl and KCl diffusion process during the salting of pre-cooked champignon mushrooms. **Food Chemistry**, 273, 99–105. https://doi.org/10.1016/J.FOODCHEM.2018.01.188

BRITO, J. G., GOMES, J. P., DA SILVA, W. P., DA SILVA E SILVA, C. M. D. P., AIRES, K. L. C. A. F., & AIRES, J. E. F. (2023). Osmotic dehydration kinetics of banana slices with peel. **Comunicata Scientiae**, 14. https://doi.org/10.14295/CS.v14.3423

CALÍN-SÁNCHEZ, Á., LIPAN, L., CANO-LAMADRID, M., KHARAGHANI, A., MASZTALERZ, K., CARBONELL-BARRACHINA, Á. A., & FIGIEL, A. (2020). Comparison of Traditional and Novel Drying Techniques and Its Effect on Quality of Fruits, Vegetables and Aromatic Herbs. **Foods**, 9(9), 1261. https://doi.org/10.3390/FOODS9091261

CARSLAW, H. S., & JAEGER, J. C. (1959). **Conduction of Heat in Solids** (2nd ed. Ox).

CRANK, J. (1979). **The mathematics of diffusion**. Oxford university press.

DA SILVA, R. C., DA SILVA, W. P., GOMES, J. P., DE MELO QUEIROZ, A. J., DE FIGUEIRÊDO, R. M. F., DE LIMA, A. G. B., ROCHA, A. P. T., DA SILVA, L. D., DE LIMA FERREIRA, J. P., DA COSTA SANTOS, D., & DE ANDRADE, R. O. (2022). A New Empirical Model for Predicting Intermittent and Continuous Drying of "Neve" Melon (Cucumis melo sp.) Seeds. **Agriculture** (Switzerland), 12(3). https://doi.org/10.3390/agriculture12030328

DA SILVA, W. P., NUNES, J. S., GOMES, J. P., DE ARAÚJO, A. C., & E SILVA, C. M. D. P. S. (2018). Description of jambolan (Syzygium cumini (L.)) anthocyanin extraction kinetics at different stirring frequencies of the medium using diffusion models. **Heat and Mass Transfer/Waerme- Und Stoffuebertragung**, 54(11). https://doi.org/10.1007/s00231-018-2349-8

DA SILVA, W. P., PRECKER, J. W., E SILVA, C. M. D. P. S., & E SILVA, D. D. P. S. (2009). Determination of the effective diffusivity via minimization of the objective function by scanning: Application to drying of cowpea. **Journal of Food Engineering**, 95(2). https://doi.org/10.1016/j.jfoodeng.2009.05.008

DE LIMA FERREIRA, J. P., DA SILVA, W. P., PAIVA, Y. F., & AMADEU, L. T. S. (2024). Impact of ultrasound pretreatment on banana chip production by convective drying using hot air: Consideration of shrinkage and variable effective mass diffusivity in the process description. **Journal of Food Process Engineering**, 47(3). https://doi.org/10.1111/jfpe.14586

GONZÁLEZ-PÉREZ, J. E., ROMO-HERNÁNDEZ, A., RAMÍREZ-CORONA, N., & LÓPEZ-MALO, A. (2022). Modeling mass transfer during osmodehydration of apple cubes with sucrose or apple juice concentrate solutions: Equilibrium estimation, diffusion model, and state observer-based approach. **Journal of Food Process Engineering**, 45(10), e14125. https://doi.org/10.1111/JFPE.14125

GONZÁLEZ PACHECO, J. I., & MALDONADO, M. B. (2024). Diffusion in biological media: a comprehensive numerical-analytical study via surface analysis and diffusivities calculation. **Scientific Reports**, 14(1), 1–18. https://doi.org/10.1038/s41598-024-67348-4

HAHN, D. W., & ÖZIŞIK, M. N. (2012). Heat Conduction: Third Edition. In **John Wiley and Sons**. John Wiley and Sons. https://doi.org/10.1002/9781118411285

JAMALI, S. H., BARDOW, A., VLUGT, T. J. H., & MOULTOS, O. A. (2020). Generalized Form for Finite-Size Corrections in Mutual Diffusion Coefficients of Multicomponent Mixtures Obtained from Equilibrium Molecular Dynamics Simulation. **Journal of Chemical Theory and Computation**, 16(6), 3799–3806. https://doi.org/10.1021/ACS.JCTC.0C00268/ASSET/IMAGES/LARGE/CT0C00268_0004.JPEG

JANOWICZ, M., CIURZYŃSKA, A., & LENART, A. (2021). Effect of Osmotic Pretreatment Combined with Vacuum Impregnation or High Pressure on the Water Diffusion Coefficients of Convection Drying: Case Study on Apples. **Foods** 2021, Vol. 10, Page 2605, 10(11), 2605. https://doi.org/10.3390/FOODS10112605

JUNQUEIRA, J. R. DE J., CORRÊA, J. L. G., DE MENDONÇA, K. S., DE MELLO JUNIOR, R. E., & SOUZA, A. U. (2021). Modeling mass transfer during osmotic dehydration of different vegetable structures under vacuum conditions. **Food Science and Technology** (Brazil), 41(2). https://doi.org/10.1590/fst.02420

KHUBBER, S., CHATURVEDI, K., TAGHI GHARIBZAHEDI, S. M., CRUZ, R. M. S., LORENZO, J. M., GEHLOT, R., & BARBA, F. J. (2020). Non-conventional osmotic solutes (honey and glycerol) improve mass transfer and extend shelf life of hot-air dried red carrots: Kinetics, quality, bioactivity, microstructure, and storage stability. **LWT**, 131. https://doi.org/10.1016/j.lwt.2020.109764

KIAN-POUR, N. (2023). Impact of Microwave-Starch-Blanching on the Drying Kinetics, Transport and Thermophysical Properties of Green Almond. **Iğdır Üniversitesi Fen Bilimleri Enstitüsü Dergisi**, 13(1). https://doi.org/10.21597/jist.1166340

KNEE, M. (2019). Rapid Measurement of Diffusion of Gas Through the Skin of Apple Fruits. **HortScience**, 26(7). https://doi.org/10.21273/hortsci.26.7.885

MACEDO, L. L., CORRÊA, J. L. G., DA SILVA ARAÚJO, C., & VIMERCATI, W. C. (2022). Effect of osmotic agent and vacuum application on mass exchange and qualitative parameters of osmotically dehydrated strawberries. **Journal of Food Processing and Preservation**, 46(7). https://doi.org/10.1111/jfpp.16621

MALDONADO, M. B., ZURITZ, C. A., & ASSOF, M. V. (2008). Diffusion of glucose and sodium chloride in green olives during curing as affected by lye treatment. **Journal of Food Engineering**, 84(2), 224--230. https://doi.org/10.1016/j.jfoodeng.2007.04.033

MALDONADO, M., & GONZÁLEZ PACHECO, J. (2020). Shrinkage phenomenon in cherries during osmotic dehydration. Annals. **Food Science and Technology**, 21(1), 19–30. http://www.afst.valahia.ro/images/documente/2020/I.2_Maldonado.pdf

MALDONADO, M., & GONZÁLEZ PACHECO, J. (2022). Mathematical modelling of mass transfer phenomena for sucrose and lactitol molecules during osmotic dehydration of cherries. **Heliyon**, 8(1), e08788. https://doi.org/10.1016/J.HELIYON.2022.E08788

MEENA, N., PRINCE, M. V., & SREEJA, R. (2022). Optimization of process parameters for ultrasound-assisted osmotic dehydration of pineapple slices using response surface methodology. **Journal of Food Processing and Preservation**, 46(9). https://doi.org/10.1111/JFPP.16507

MUGI, V. R., & CHANDRAMOHAN, V. P. (2021). Shrinkage, effective diffusion coefficient, surface transfer coefficients and their factors during solar drying of food products – A review. **Solar Energy**, 229. https://doi.org/10.1016/j.solener.2021.07.042

OLADZADABBASABADI, N., MOHAMMADI NAFCHI, A., GHASEMLOU, M., ARIFFIN, F., SINGH, Z., & AL-HASSAN, A. A. (2022). Natural anthocyanins: Sources, extraction, characterization, and suitability for smart packaging. **Food Packaging and Shelf Life**, 33, 100872. https://doi.org/10.1016/J.FPSL.2022.100872

PANDISELVAM, R., TAK, Y., OLUM, E., SUJAYASREE, O. J., TEKGÜL, Y., ÇALIŞKAN KOÇ, G., KAUR, M., NAYI, P., KOTHAKOTA, A., & KUMAR, M. (2021). Advanced osmotic dehydration techniques combined with emerging drying methods for sustainable food production: Impact on bioactive components, texture, color, and sensory properties of food. **Journal of Texture Studies**. https://doi.org/10.1111/JTXS.12643

PEREIRA, M. T. L., DE OLIVEIRA FARIAS, V. S., DA SILVA JÚNIOR, A. F., DO NASCIMENTO LIMA, A. R., VIEIRA, V. B., DE MEDEIROS, R. A., DA SILVA, W. P., FRANCO, C. M. R., & DE ATAÍDE, J. S. P. (2023). Analysis of drying of melon peels using numerical solution of the diffusion equation. **Journal of Food Process Engineering**, 46(3). https://doi.org/10.1111/jfpe.14267

PINHEIRO, M. N. C., & CASTRO, L. M. M. N. (2023). Effective moisture diffusivity prediction in two Portuguese fruit cultivars (Bravo de Esmolfe apple and Madeira banana) using drying kinetics data. **Heliyon**, 9(7). https://doi.org/10.1016/j.heliyon.2023.e17741

SALEHI, F., CHERAGHI, R., & RASOULI, M. (2022). Mass transfer kinetics (soluble solids gain and water loss) of ultrasound-assisted osmotic dehydration of apple slices. **Scientific Reports**, 12(1). https://doi.org/10.1038/s41598-022-19826-w

SALEHI, F., CHERAGHI, R., & RASOULI, M. (2023). Mass transfer analysis and kinetic modeling of ultrasound-assisted osmotic dehydration of kiwifruit slices. **Scientific Reports**, 13(1). https://doi.org/10.1038/s41598-023-39146-x

SAYAGO, U. F. C. (2021). Design and development of a biotreatment of E. crassipes for the decontamination of water with Chromium (VI). **Scientific Reports**, 11(1). https://doi.org/10.1038/s41598-021-88261-0

SULISTYAWATI, I., VERKERK, R., FOGLIANO, V., & DEKKER, M. (2020). Modelling the kinetics of osmotic dehydration of mango: Optimizing process conditions and pre-treatment for health aspects. **Journal of Food Engineering**, 280, 109985. https://doi.org/10.1016/J.JFOODENG.2020.109985

ZECCHI, B., & GERLA, P. (2020). Effective diffusion coefficients and mass flux ratio during osmotic dehydration considering real shape and shrinkage. **Journal of Food Engineering**, 274. https://doi.org/10.1016/j.jfoodeng.2019.109821

ZURITZ, C. A., & MALDONADO, M. B. (2004). A simple method to determine diffusion of sodium in the epidermis of green olives. **Journal of Food Process Engineering**, 27(5), 328--344. https://doi.org/10.1111/j.1745–4530.2004.00466.x.

SOBRE O ORGANIZADOR

Alireza Mohebi Ashtiani possui graduação em bacharelado em Matemática, Matemática Aplicada, pela Amirkabir University of Technology (Polytechnic of Tehran), Teerã/Irã (2003), mestrado em Matemática Aplicada pelo Institute for Advanced Studies in Basic Siences (IASBS), Zanjan/Irã (2005) e doutorado em Engenharia Elétrica pela Universidade Estadual de Campinas (UNICAMP) na área de Automação (2012). Foi bolsista de Pós-doutorado Júnior do CNPq no Instituto de Matemática, Estatística e Computação Científica (IMECC/UNICAMP) e bolsista de Pós-doutorado da Fundação de Amparo à Pesquisa do Estado de São Paulo (FAPESP) na Faculdade de Ciências Aplicadas da Universidade Estadual de Campinas (FCA/UNICAMP). Desde 2013 é docente vinculado ao Departamento Acadêmico de Matemática do Campus Londrina da Universidade Tecnológica Federal do Paraná (UTFPR), e atualmente, docente permanente do Programa de Pós-Graduação em Matemática em Rede Nacional (PROFMAT) da UTFPR, Campus Cornélio Procópio.

Alireza Mohebi Ashtiani
http://lattes.cnpq.br/5025709771742662

ÍNDICE REMISSIVO